Structural and morphological studies of ZnO nanostructures

A. M. Mohammad[a,*], H. S. Ahmed Al-Jaf [a], H. Sh. Ahmed[a], M. M. Mohammed[b], Z. T. Khodair[c]
[a]*University of Garmian, College of Education, Department of Physics, Kurdistan region, Iraq*
[b]*University of Garmian, College of Education, Department of Chemistry, Kurdistan region, Iraq*
[c]*University of Diyala, College of Science, Department of Physics, Diyala, Iraq*

Zinc oxide (ZnO) nanostructures were manufactured successfully using the sol-gel approach in this study. The impact of calcination temperatures on their structural and morphological properties is studied using three different calcination temperatures (350, 400, and 450 °C). XRD, FE-SEM, EDS, and a Raman scattering spectroscope were used to characterize the samples. In all samples, X-ray diffraction (XRD) of calcined samples (350-450 °C) reveals the presence of the wurtzite hexagonal nanocrystalline structure of ZnO compound. The XRD patterns showed no additional peaks, indicating that the final product is exclusively ZnO nanostructures. The FE-SEM pictures of a calcined ZnO sample at 450°C revealed a porous structure, longer length and diameter, and agglomeration of mixed polyhedral shape particles as the calcination temperature increased. The presence of necessary oxide material in the EDS spectrum confirmed the synthesis of ZnO, indicating that the purity of ZnO was appropriate. Finally, using Raman spectroscopy, the vibrational characteristics of ZnO were studied. Several bands in Raman spectra appeared to belong to ZnO vibrational modes, confirming the purity of the produced ZnO samples. The findings of such a study were presented in this paper.

(Received February 28, 2022; Accepted June 9, 2022)

Keywords: ZnO nanostructures, Calcination, Sol-gel, XRD, FE-SEM, Raman spectroscopy

1. Introduction

The field of nanotechnology is rapidly evolving. Herein, Humanity is taking advantage from this rapid development and this opened a new potential and broader perspective to the world [1, 2]. All of this has been accomplished by manipulating materials at the nanoscale level with precise chemical composition, size, and shape control, which has found applications in a variety of disciplines due to their unique chemical, physical, and biological properties [3, 4]. Zinc Oxide has already received a lot of attention. The fact that the excitation state of Zinc Oxide is stable at room temperature has prompted scientists and researchers to pay close attention to it, especially given the potential benefits of ZnO such as wide band gaps (3.37 eV) and high exitonic binding energy (60 meV)[5]. Leukemia and cancer have both been treated using zinc oxide. ZnO has been shown to have high bactericidal activity against a wide range of microorganisms in previous antibacterial studies [6]. Zinc oxide is used in a variety of fields, including cosmetics, gas sensors, agriculture, photocatalysis, transparent conductors, biomedical devices, and healthcare items [7-9]. Microemulsion [10], solid-state reaction [11], hydrothermal [12], sol-gel [13], co-precipitation [14], and other methods have been proposed to synthesize metal oxide nanostructures. Furthermore, a method for extracting ZnO nanoparticles from plants that is both practical and environmentally acceptable has been proposed and is gaining traction [4, 15]. However, employing nitrates as a source of metallic ions and harmless materials as a size-limiting agent, the sol-gel technique has proven to be a suitable method for obtaining high-purity, low-cost crystalline powders with strong homogeneity control. In comparison to other traditional procedures, the sol–

* Corresponding author: ali.mustafa@garmian.edu.krd
https://doi.org/10.15251/JOR.2022.183.443

gel approach is preferred for the preparation of metal oxide composites[16]. The production of ZnO nanostructures utilizing $Zn(NO_3)_2.6H_2O$ as a zinc source is described here using a sol-gel approach. Using X-ray diffraction, field emission scanning electron microscopy, and Raman spectroscopy, the influence of calcination temperature on the structural and morphological of synthesized ZnO was investigated.

2. Experimental details

2.1. Sample synthesis

The sol-gel approach was used to make ZnO nanostructures that were calcined at varied temperatures. A stoichiometric amount of Zn nitrates $Zn(NO_3)_2 \cdot 6H_2O$ was weighed and completely dissolved in minimum amount of de-water while stirring constantly until a translucent solution was obtained. The pH of the final solution was then raised to 7 by adding ammonia solution drop by drop [17], and the temperature of the hot plate was raised to 90-100 °C with continuous stirring to uniformly mix the solution. As a result, the solution was evaporated, and all of the water was removed, yielding a dried precursor [18]. To investigate the influence of calcination on structural and morphological qualities, the powder was crushed in a mortar and calcined in air for 3 hours at varied temperatures of 350, 400, and 450 °C in a research oven.

2.2. Characterizations

The crystalline phase and identification of synthesized powders were determined using X-Ray Diffraction (XRD), model PANalytical (X'pert Pro, Netherlands) equipped with Cu kα radiation source (λ = 1.5406 Å). At room temperature, field emission scanning electron microscopy (FE-SEM; Model Mira3-XMU, TESCAN, Japan) was used to evaluate the surface morphology. To establish the phase of ZnO and study the vibrational spectra of all samples, Raman spectroscopy (Micro-Raman spectroscopy-785 nm laser) was utilized.

3. Results and discussion

3.1. XRD studies

The sharpness of the XRD peaks (Fig. 1) revealed the characteristic patterns, strong crystallinity, and confirmed the production of crystalline ZnO samples at calcination temperatures (350, 400, and 450 °C for 3 h).

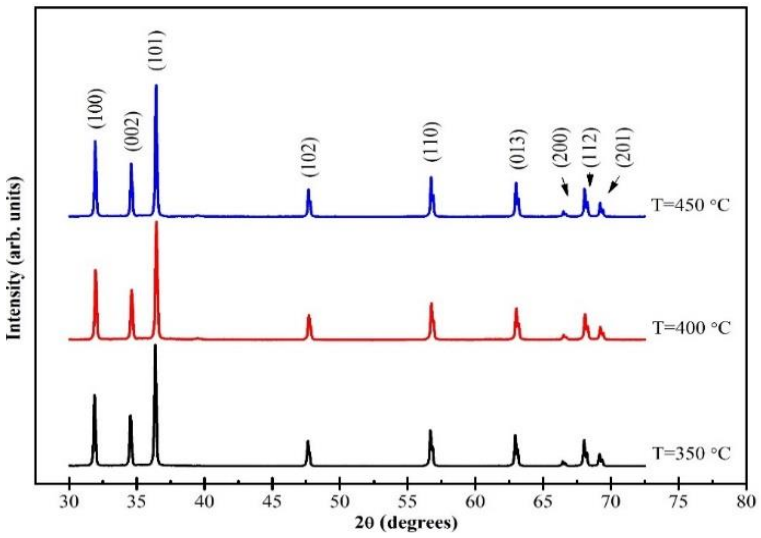

Fig. 1. XRD patterns of calcined ZnO samples at 350,400 and 450 °C.

The three strongest diffraction peaks at an angle of 2θ are indexed with miller indices (100), (002), and (101), indicating high phase crystallinity, and correspond to the hexagonal wurtzite phase of ZnO nanostructure (space group P63mc, ICDD Card No.98-010-8249). This finding is consistent with that of Davood and Taha [19] and Ismail et al. [20]. It was clearly noticed that as the calcination temperature was increased, the distinctive peaks got higher and sharper, indicating an enhancement of crystallinity nature due to agglomeration, implying that the crystallinity had improved [21, 22]. Importantly, no extra peaks relating to impurities were found, indicating that the final product is exclusively ZnO nanostructures.

The lattice parameters '*a*' and '*c*' of the ZnO nanostructures were calculated using the following equations [23, 24].

$$\frac{1}{d^2} = \frac{4}{3}\left(\frac{h^2 + hk + k^2}{a^2}\right) + \frac{l^2}{c^2} \tag{1}$$

$$a = \frac{\lambda}{\sqrt{3}\sin\theta_{100}} \tag{2}$$

$$c = \frac{\lambda}{\sin\theta_{002}} \tag{3}$$

where *a* and *c* are the lattice parameters, (*hkl*) are the Miller indices, *d* is an interplanar distance, λ is the X-ray wavelength (1.5406 Å for CuK_α radiation) and θ is Bragg diffraction angle. Table 1 shows the lattice characteristics of the calcined samples at various temperatures, which reveal hexagonal structure. The lattice parameters '*a*' and '*b*' were found to decrease with increasing calcination temperature (350 and 400 °C), then increase at (450 °C). The presence of point defects and oxygen vacancies is confirmed by the observation of small differences in the lattice parameters values compared to standard values, which could be attributable to calcination temperature [25]. Literatures [25, 26] have reported similar fluctuations in lattice parameter.

Table 1. The diffraction angle (2θ), lattice parameters (a, c and c/a), crystallite size (D), dislocation density (δ) and micro-strain (ε) of calcined ZnO samples at 350,400 and 450 °C.

Temperature °C	2θ (deg)	Lattice parameter			*D*(nm)	δ (nm^{-2}) $\times10^{-4}$	$\varepsilon\times10^{-4}$
		a (Å)	*c* (Å)	*c/a*			
350	36.3619	3.239	5.190	1.602	59.725	2.803	5.804
400	36.4313	3.232	5.180	1.603	64.332	2.416	5.388
450	36.4132	3.234	5.183	1.603	75.340	1.762	4.601

According to the XRD data, The average crystallite size (*D*) was estimated using the Scherrer formula as follows [27, 28].

$$D = \frac{0.9\,\lambda}{\beta\,cos\theta} \tag{4}$$

where β is the full width at half maximum (FWHM). With increasing calcination temperature from 350 to 450 °C, the average crystallite size (*D*) was observed to grow from 59.725 to 75.340 nm (Table 1). This could be linked to an increase in crystal growth rate as a result of volume expansion and a decrease in system supersaturation at high temperatures [29]. The particle size *D* can be used to calculate the dislocation density (δ), which is a measure of the number of defects and vacancies in the crystal [30].

$$\delta = \frac{1}{D^2} \tag{4}$$

The dislocation density (δ) is inversely related to crystallite size, as shown in table 1, and its value falls as the calcination temperature rises. The following formula [31] was used to calculate the material's micro-strain (ε).

$$\varepsilon = \frac{\beta \cos\theta}{4} \tag{4}$$

The micro-strain (ε) reduces as the calcination temperature rises (Table 1), indicating that both (D) and (ε) are calcination temperature dependent. As previously stated by A.A. Othman et al.[32], the reduction in micro-strain may be the primary cause of improved crystallinity.

Table 2. The unit cell volume (V), X-ray density (ρ), atomic packing fraction (APF), bond length (L), Young modulus (Y), energy density (u) and stress (σ) of calcined ZnO samples at 350,400 and 450 °C.

Temperature °C	V (Å)^3	ρ(g/cm^3)	*APF*	$L\times10^{-10}$ (m)	$Y\times10^9$ (Pa)	$u\times10^3$ (J/m^3)	$\sigma \times 10^9$ (Pa)
350	47.173	5.728	0.755	1.972	224.529	37.814	0.1303
400	46.858	5.767	0.754	1.967	224.380	32.570	0.1209
450	46.954	5.755	0.754	1.968	224.391	23.749	0.1032

The volume of unit cell (V) was calculated by the following equation [33].

$$V = \frac{\sqrt{3}}{2} a^2 c \tag{5}$$

The lattice parameters 'a' and 'c' of ZnO calcined at 350 °C are clearly larger, resulting in a bigger unit cell volume (V). This trend is consistent with Pradeev et al. [34], who found that when the calcination temperature rises, the diffraction angle shifts to lower 2θ values, increasing the volume of the unit cell. Table 1 and Fig 2 demonstrate that as the calcination temperature rises, the volume of the unit cell decreases from 47.173 Å^3 to 46.858 Å^3 and then rises to 46.954 Å^3, corresponding to an increase in 2θ from 36.3619 to 36.4313 and subsequently decreases to 36.4132.

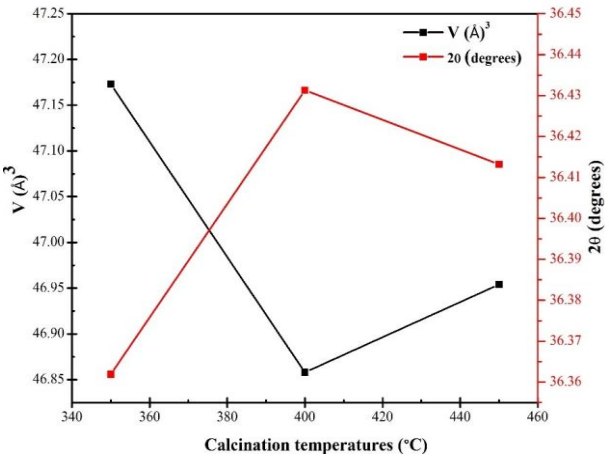

Fig. 2. Dependence of the unit cell volume and diffraction angle on calcination temperature (350,400 and 450 °C).

The atomic packing fraction (*APF*) and X-ray density (ρ) of ZnO were calculated using the equations below [35, 36].

$$\rho_x = \frac{nM}{N_A V} \tag{6}$$

$$APF = \frac{2\pi a}{3\sqrt{3}c} \tag{7}$$

where, n is the number of atoms per unit cell, M is molecular weight, N_A is Avogadro's number and V is the volume of the unit cell. The X-ray density and atomic packing fraction do not differ considerably as the calcination temperature rises. The relationship [37] is used to calculate the bond length (L) of Zn–O.

$$L = \sqrt{\frac{a^2}{3} + \left(\frac{1}{2} - u\right)^2 c^2} \tag{8}$$

where (u) is the positional parameter for the wurtzite structure and given by.

$$u = \frac{a^2}{3c^2} + 0.25 \tag{9}$$

Table 2 shows the bond length values calculated for Zn-O powders. These findings are quite similar to those seen in previous studies [20, 38]. Young's modulus (Y_{hkl}) for hexagonal crystal were calculated by the following equations [31].

$$Y_{hkl} = \frac{\left[h^2 + \frac{(h+2k)^2}{3} + \left(\frac{al}{c}\right)^2\right]^2}{S_{11}\left(h^2 + \frac{(h+2k)^2}{3}\right)^2 + S_{33}\left(\frac{al}{c}\right)^4 + (2S_{11} + S_{44})\left(h^2 + \frac{(h+2k)^2}{3}\right)\left(\frac{al}{c}\right)^2} \tag{10}$$

The values of S_{11}, S_{13}, S_{33} and S_{44} which represent the elastic compliances of ZnO are 7.858×10^{-12}, 2.206×10^{-12}, 6.940×10^{-12} and 23.57×10^{-12} m^2 N^{-1} respectively [39]. The following relation can calculate the energy per unit volume (U) as a function of strain (ε) of a lattice.

$$U = \frac{(\varepsilon^2 Y_{hkl})}{2} \tag{11}$$

The stress (σ) can be given by Hook's law.

$$\sigma = \varepsilon Y \tag{12}$$

The parameters of Young's modulus (Y_{hkl}) (Table 2) and internal strain (ε) determine the energy density (U). It was discovered that as the calcination temperature rises, the energy density falls. The declines are due to a reduction in internal strain (Table 1). As a result, the stress (σ) values drop, and this behavior is consistent with that seen by P. Shunmuga Sundaram et al. [31].

3.2. Morphology studies

The surface morphology and EDS spectrum of produced ZnO samples at various calcination temperatures were studied using the FE-SEM technique at room temperature, as shown in Fig. 3 (a-c). The diameter of the ZnO particles is substantially bigger than the crystallite size determined by XRD measurement. The micron-sized particles visible in FE-SEM pictures are thought to be made up of a large number of original nanocrystallites discovered by XRD. The micrographs of ZnO nanostructure are influenced by increasing calcination temperature and have a porous structure with a high agglomeration of plate-like and polyhedral shape particles, as seen in the photos. At a higher calcination temperature (450 C), however, the nanostructures particles agglomerated and formed bigger particle sizes. The fusion of nearby particles together, which

may be the major reason for the rise in particle size by melting their surfaces, may be related to the increase in particle size with an increase in calcination temperature [40]. This increased particle aggregation is thought to be caused by the high surface energy of the ZnO nanostructure [24].

Energy dispersive spectrum EDS analysis was used to determine uniformity and material composition. The presence of the necessary oxide materials in an EDS spectrum suggested sufficient purity of ZnO, and the principal constituents of the manufactured material are Zn and O, with unwanted precursors such as nitrate ions totally eliminated from the final product. Fig. 3 shows the weight percentages of elemental elements in all samples (a-c).

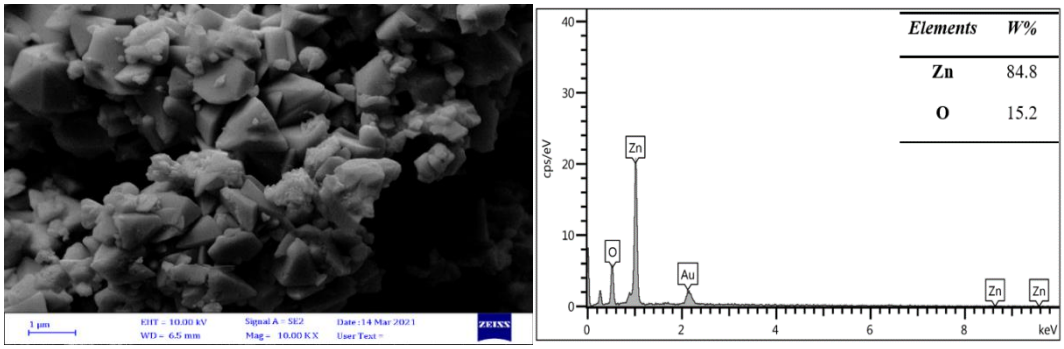

(a)

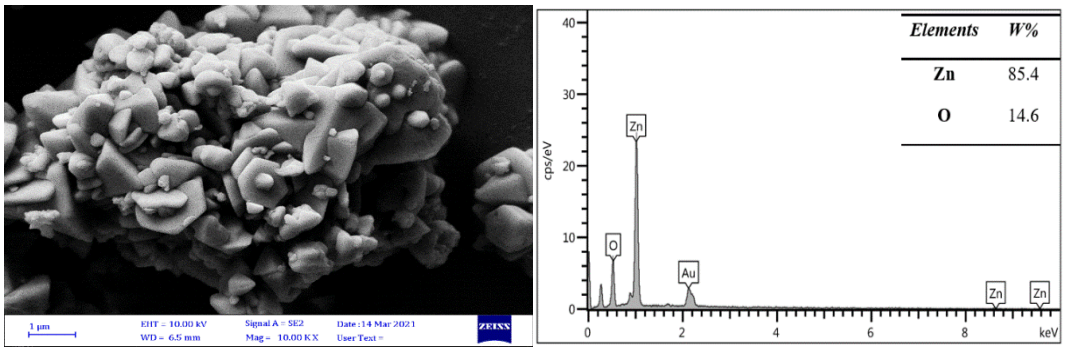

(b)

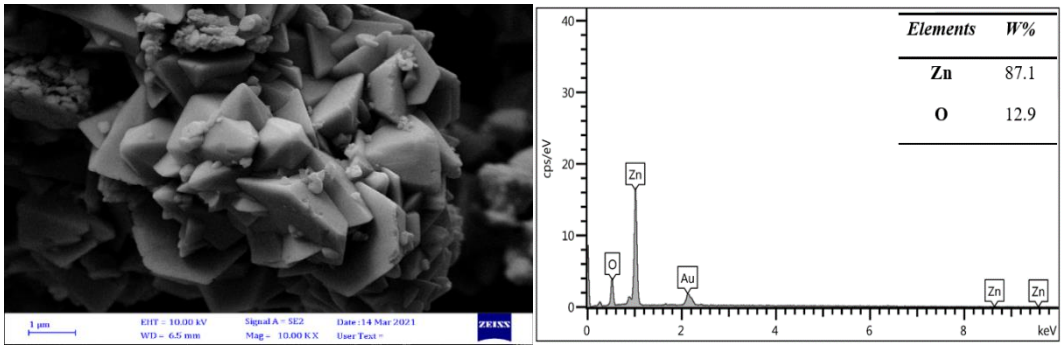

(c)

Fig. 3. FE-SEM image and EDS spectrum of calcined ZnO samples (a) calcined at 350 °C, (b) calcined at 400 °C and (c) calcined at 450 °C.

3.3. Raman spectral studies

The Raman scattering spectroscope is a useful tool that works by measuring the change in photon frequency that occurs when monochromic light interacts with a specimen. It provides

information on the structure of nanomaterials as well as vibrations caused by imperfections. Raman spectra at 785 nm excitation wavelength at room temperature were used to characterize ZnO nanostructures. The ZnO wurtzite-phase has two formula units per primitive unit cell and belongs to the space group P63mc. $2A_1+2E_1+2B_1+2E_2$ are the irreducible representations at the zone center [41]. The acoustic phonons are represented by the A_1 and E_1 modes, whereas the optical phonons are represented by the remaining modes. The A_1 and E_1 modes are polar in character, exhibit varied frequencies, and can be split into the transverse-optical (TO) and longitudinal-optical (LO) phonons. Except for B_1, all of these modes are Raman active. The non-polar E_2 modes, on the other hand, have two modes with two frequencies, E_2 (high) connected to oxygen displacement and E_2 (low) related to the Zn sub lattice, and are exclusively Raman active [27, 42].

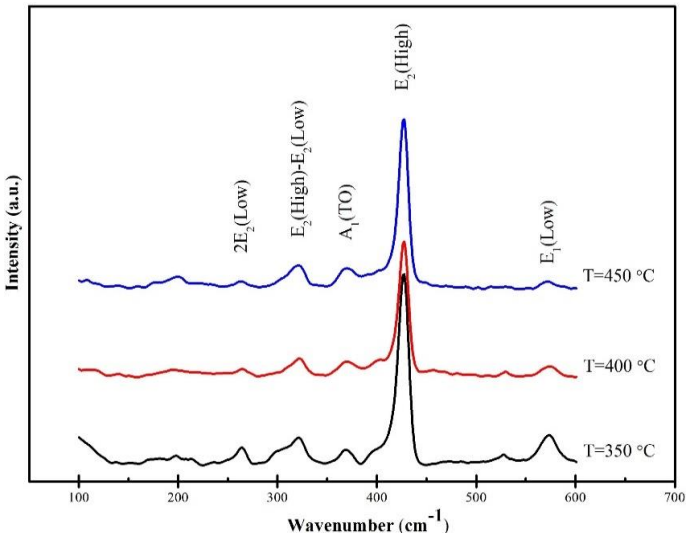

Fig. 4. Raman spectrum of calcined ZnO samples at 350,400 and 450 °C.

Fig. 4 shows the characteristic Raman spectra of ZnO nanostructures at room temperature. The spectra show all of the Raman characteristic bands of ZnO in the range of 100-600 cm^{-1}. Raman spectra reveal ZnO vibrational modes in several bands, confirming the preparation of pure ZnO nanostructure. The nonpolar optical phonon vibration mode E_2 (high) of oxygen sub-lattice is attributable to the occurrence of a powerful, acute, and dominant peak at 427.504 cm^{-1} for all calcined samples at 350, 400, and 450 °C. Low intensity pecks at 321.323, 322.571, and 321.323 cm^{-1} for calcined materials at 300, 350, 400, and 450 °C are attributable to the second-order Raman mode coming from zone boundary phonons of the hexagonal wurtzite ZnO. The E_1 longitudinal optical phonons mode of hexagonal ZnO is represented by the peaks at 573.916, 573.916, and 571.554 cm^{-1} at different calcination temperatures. The production of defects (oxygen vacancies or zinc interstitials) is thought to be the cause of the produced peak at E_1 (LO) mode [43]. For varying calcination temperatures, the peaks at (368.545, 369.782, and 369.782 cm^{-1}) correspond to A_1 transverse optical (TO) modes, respectively.

4. Conclusions

The crystal structure of ZnO nanostructures synthesized by sol-gel approach at different calcination temperatures (350, 400, and 450 °C). The obtained Zinc oxide was investigated to see if structural and morphological qualities were affected by calcination temperature. Without any secondary phases, the XRD investigation revealed the nanocrystalline hexagonal wurtzite structure with space group P63mc. The size of typical crystallites has increased as the calcination temperature has increased. Temperature affects the other properties in both a regulated and

unregulated manner. Morphological analysis using FE-SEM images reveals that each sample has nearly identical surface morphology, with increasing length, diameter, and agglomeration of plate-like and polyhedral form particles as the calcination temperature rises. The EDS spectra confirmed the synthesis of ZnO in all of the calcined samples and the presence of Zn and O as the main components. The undesirable precursors, such as nitrate ions, are completely eliminated. The presence of distinctive ZnO bands in the range of 100-600 cm^{-1} is indicated by the peaks on the Raman spectra. These bands exhibit ZnO vibrational modes, indicating that pure ZnO nanostructures have been created.

Acknowledgements

The authors are grateful to the University of Garmian, College of Eduatuion, Department of Physics in Kurdistan region, Iraq, and the center of DeyPetronic co., Tehran, Iran to assist them in completing the practical portion of this research, as well as laboratory tests.

References

[1] D. M. Cruz, E. Mostafavi, A. Vernet-Crua, H. Barabadi, V. Shah, J. L. Cholula-Díaz, G. Guisbiers, and T. J. Webster, Journal of Physics: Materials, vol. 3, no. 3, pp. 034005, 2020; https://doi.org/10.1088/2515-7639/ab8186

[2] V. Kalpana, and V. Devi Rajeswari, Bioinorganic chemistry and applications, vol. 2018, 2018; https://doi.org/10.1155/2018/3569758

[3] A. Jaramillo, R. Baez-Cruz, L. Montoya, C. Medinam, E. Pérez-Tijerina, F. Salazar, D. Rojas, and M. Melendrez, Ceramics International, vol. 43, no. 15, pp. 11838-11847, 2017; https://doi.org/10.1016/j.ceramint.2017.06.027

[4] W. Ahmad, and D. Kalra, Journal of King Saud University-Science, vol. 32, no. 4, pp. 2358-2364, 2020; https://doi.org/10.1016/j.jksus.2020.03.014

[5] S. Hingorani, V. Pillai, P. Kumar, M. Multani, and D. Shah, Materials Research Bulletin, vol. 28, no. 12, pp. 1303-1310, 1993; https://doi.org/10.1016/0025-5408(93)90178-G

[6] J. Sawai, Journal of microbiological methods, vol. 54, no. 2, pp. 177-182, 2003; https://doi.org/10.1016/S0167-7012(03)00037-X

[7] E. T. Bekele, B. A. Gonfa, O. A. Zelekew, H. H. Belay, and F. K. Sabir, Journal of Nanomaterials, vol. 2020, 2020; https://doi.org/10.1155/2020/2817037

[8] M. Mauricio, S. Guerra-Ojeda, P. Marchio, S. Valles, M. Aldasoro, I. Escribano-Lopez, J. Herance, M. Rocha, J. Vila, and V. Victor, Oxidative Medicine and Cellular Longevity, vol. 2018, 2018; https://doi.org/10.1155/2018/6231482

[9] S. Vijayakumar, B. Vaseeharan, B. Malaikozhundan, and M. Shobiya, Biomedicine & Pharmacotherapy, vol. 84, pp. 1213-1222, 2016; https://doi.org/10.1016/j.biopha.2016.10.038

[10] M. Emsaki, S. Hassanzadeh-Tabrizi, and A. Saffar-Teluri, Journal of Materials Science: Materials in Electronics, vol. 29, no. 3, pp. 2384-2391, 2018; https://doi.org/10.1007/s10854-017-8157-y

[11] B. Arunkumar, J. Vasudevan, S. J. Jeyakumar, and M. Jothibas, Materials Today: Proceedings, 2021; https://doi.org/10.1016/j.matpr.2021.08.012

[12] S. Agarwal, P. Rai, E. N. Gatell, E. Llobet, F. Güell, M. Kumar, and K. Awasthi, Sensors and Actuators B: Chemical, vol. 292, pp. 24-31, 2019; https://doi.org/10.1016/j.snb.2019.04.083

[13] S. Demirci, T. Dikici, M. M. Tünçay, and N. Kaya, Applied Surface Science, vol. 507, pp. 145083, 2020; https://doi.org/10.1016/j.apsusc.2019.145083

[14] R. E. Adam, G. Pozina, M. Willander, and O. Nur, Photonics and Nanostructures-Fundamentals and Applications, vol. 32, pp. 11-18, 2018; https://doi.org/10.1016/j.photonics.2018.08.005

[15] M. Nilavukkarasi, S. Vijayakumar, and S. Prathipkumar, Materials Science for Energy Technologies, vol. 3, pp. 335-343, 2020; https://doi.org/10.1016/j.mset.2019.12.004

[16] G. De, G. Mattei, P. Mazzoldi, C. Sada, G. Battaglin, and A. Quaranta, Chemistry of materials, vol. 12, no. 8, pp. 2157-2160, 2000; https://doi.org/10.1021/cm001053i

[17] Z. T. Khodair, A. M. Mohammad, and A. A. Khadom, Chemical Data Collections, vol. 25, pp. 100315, 2020; https://doi.org/10.1016/j.cdc.2019.100315

[18] D. Zhang, J. Li, H. Zhang, Y. Wu, Q. Li, and G. Ma, Applied Physics A, vol. 122, no. 4, pp. 306, 2016; https://doi.org/10.1007/s00339-016-9845-9

[19] D. Raoufi, and T. Raoufi, Applied surface science, vol. 255, no. 11, pp. 5812-5817, 2009; https://doi.org/10.1016/j.apsusc.2009.01.010

[20] M. Ismail, K. Taha, A. Modwi, and L. Khezami, "ZnO nanoparticles: Surface and X-ray profile analysis," J. Ovonic Res, vol. 14, pp. 381-393, 2018.

[21] H. Mehranfar, M. Mohammed, A. Mohammad, Journal of Non-Oxide Glasses Vol, vol. 11, no. 3, pp. 33-40, 2019.

[22] A. M. Mohammad, S. M. A. Ridha, and T. H. Mubarak, "Dielectric properties of Cr-substituted cobalt ferrite nanoparticles synthesis by citrate-gel auto combustion method," International Journal of Applied Engineering Research, vol. 13, no. 8, pp. 6026-6035, 2018.

[23] J. Bezerra, R. Matos, B. Zucolotto, P. Pedra, and N. Ferreira, Materials Science and Technology, vol. 35, no. 2, pp. 231-239, 2019; https://doi.org/10.1080/02670836.2018.1558598

[24] D. Raoufi, Renewable Energy, vol. 50, pp. 932-937, 2013; https://doi.org/10.1016/j.renene.2012.08.076

[25] A. Bhosale, K. Abitkar, P. Sadalage, K. Pawar, and K. Garadkar, Journal of Materials Science: Materials in Electronics, vol. 32, no. 15, pp. 20510-20524, 2021; https://doi.org/10.1007/s10854-021-06563-5

[26] U. Seetawan, S. Jugsujinda, T. Seetawan, A. Ratchasin, C. Euvananont, C. Junin, C. Thanachayanont, and P. Chainaronk, Mater Sci Appl, vol. 2, no. 09, pp. 1302, 2011; https://doi.org/10.4236/msa.2011.29176

[27] A. J. Reddy, M. Kokila, H. Nagabhushana, J. Rao, C. Shivakumara, B. Nagabhushana, and R. Chakradhar, Spectrochimica Acta Part A: Molecular and Biomolecular Spectroscopy, vol. 81, no. 1, pp. 53-58, 2011; https://doi.org/10.1016/j.saa.2011.05.043

[28] A. M. Mohammad, International Journal of Nanoelectronics & Materials, vol. 13, no. 2, 2020.

[29] C. H. Chia, S. Zakaria, M. Yusoff, S. Goh, C. Y. Haw, S. Ahmadi, N. M. Huang, and H. N. Lim, Ceramics International, vol. 36, no. 2, pp. 605-609, 2010; https://doi.org/10.1016/j.ceramint.2009.10.001

[30] M. Sathya, and K. Pushpanathan, Applied Surface Science, vol. 449, pp. 346-357, 2018; https://doi.org/10.1016/j.apsusc.2017.11.127

[31] P. S. Sundaram, S. S. R. Inbanathan, and G. Arivazhagan, Physica B: Condensed Matter, vol. 574, pp. 411668, 2019; https://doi.org/10.1016/j.physb.2019.411668

[32] A. Othman, M. Osman, E. Ibrahim, and M. A. Ali, Ceramics International, vol. 43, no. 1, pp. 527-533, 2017; https://doi.org/10.1016/j.ceramint.2016.09.189

[33] A. K. Zak, W. A. Majid, M. E. Abrishami, and R. Yousefi, Solid State Sciences, vol. 13, no. 1, pp. 251-256, 2011; https://doi.org/10.1016/j.solidstatesciences.2010.11.024

[34] K. P. Raj, and K. Sadayandi, Physica B: Condensed Matter, vol. 487, pp. 1-7, 2016; https://doi.org/10.1016/j.physb.2016.01.020

[35] S. Li, H. Zhang, S. Leng, Z. Yang, J. Shao, and Z. Li, Journal of Materials Science: Materials in Electronics, vol. 29, no. 13, pp. 10969-10975, 2018; https://doi.org/10.1007/s10854-018-9178-x

[36] V. Mote, J. Dargad, and B. Dole, " Nanoscience and Nanoengineering, vol. 1, no. 2, pp. 116-122, 2013; https://doi.org/10.13189/nn.2013.010204

[37] P. Bindu, and S. Thomas, Journal of Theoretical and Applied Physics, vol. 8, no. 4, pp. 123-134, 2014; https://doi.org/10.1007/s40094-014-0141-9

[38] A. Modwi, M. Abbo, E. Hassan, K. Taha, L. Khezami, and A. Houas, " Journal of Ovonic

research, vol. 12, no. 2, 2016.
[39] B. Rajesh Kumar, and B. Hymavathi, Journal of Asian Ceramic Societies, vol. 5, no. 2, pp. 94-103, 2017; https://doi.org/10.1016/j.jascer.2017.02.001
[40] A. Mohammad, M. Mohammed, and L. Hussein, Digest Journal of Nanomaterials and Biostructures, vol. 15, no. 1, pp. 231-241, 2020.
[41] J. Guo, and C. Peng, Ceramics International, vol. 41, no. 2, pp. 2180-2186, 2015; https://doi.org/10.1016/j.ceramint.2014.10.017
[42] J. Singh, S. Sharma, S. Soni, S. Sharma, and R. C. Singh, Materials Science in Semiconductor Processing, vol. 98, pp. 29-38, 2019; https://doi.org/10.1016/j.mssp.2019.03.026
[43] A. Kamalianfar, S. Halim, M. G. Naseri, M. Navasery, F. U. Din, J. Zahedi, K. Behzad, K. Lim, A. L. Monghadam, and S. Chen, Chinese Physics B, vol. 22, no. 8, pp. 088103, 2013; https://doi.org/10.1088/1674-1056/22/8/088103